Optical and Quantum Electronics **23** *(1991) 685–702*

Theoretical analysis of pulse shaping of self-phase modulated pulses in a grating pair compressor

A. PENZKOFER
Naturwissenschaftliche Fakultät II – Physik, Universität Regensburg, W-8400 Regensburg, Germany

Received 30 July; revised 19 December 1990; accepted 21 January 1991

The intracavity self-phase modulation in a picosecond Nd:glass laser and the external pulse compression in a grating pair arrangement is simulated. Fast-Fourier transforms are applied for the determination of the frequency spectra caused by self-phase modulation and the temporal shapes caused by grating pair pulse compression. The calculations are compared with recently reported experimental results.

1. Introduction

The frequency chirping of pico- and femtosecond light pulses by self-phase modulation and the subsequent temporal shaping by pulse passage through dispersive elements is widely applied for. Frequency up-chirped (positive chirped) pulses are shortened temporally in grating pair or prism pair compressors [1, 2] and broadened temporally in grating pair pulse stretchers [3, 4]. Frequency down-chirped (negative chirped) pulses are broadened in conventional compressors and are shortened in conventional stretchers. Insertion of spatial filters or phase filters in the dispersive arrangements offers a wide range of pulse reshaping [5, 6]. Besides dispersive pulse compression by spectral phase changing, spectral bandwidth limitations in gain media or transmission bandpass filters act pulse shortening on frequency chirped pulses by spectral amplitude changing [7–12].

In pulsed working solid-state mode-locked lasers the pulses become intracavity self-phase modulated by the multiple transits through the gain medium (see [7, 13, 14] and references therein). Intracavity self-phase modulation is also observed in the regenerative amplification of weak input pulses from c.w. mode-locked lasers [15]. Pico- and subpicosecond pulses generated in c.w. mode-locked lasers are often self-phase modulated externally in optical fibres [1, 2, 16, 17]. In long fibres self-phase modulation and group velocity dispersion occur simultaneously. The combined effect of positive self-phase modulation (nonlinear refractive index coefficient $n_2 > 0$) and normal group velocity dispersion ($\partial^2 n/\partial\lambda^2 > 0$) gives a nearly linear frequency up-chirp (positive chirp $\partial\nu/\partial t > 0$, ν being the instantaneous frequency). In the anomalous group velocity dispersion region of optical fibres (wavelength typically around 1.5 μm [18]) the combined effects of positive self-phase modulation and dispersion leads to soliton propagation [1, 2, 16–18]. In c.w. mode-locked femtosecond dye lasers group velocity dispersion and self-phase modulation occur in the gain and loss jets. Prism combinations [19], Gires–Tournois interferometers [20] and special

0306-8919/91 $03.00 + .12

mirrors [21] have been applied to compensate the group velocity dispersion and to compress the frequency chirped pulses.

In a recent experiment we compressed intracavity self-phase modulated pulses of an actively and passively mode-locked pulsed Nd:glass laser in an external grating pair compressor [22]. Around and slightly beyond the pulse train maximum the intracavity self-phase modulation broadened the pulses of 5 ± 1 ps duration to a spectral width of $60 \pm 20\,\mathrm{cm}^{-1}$. These pulses could be compressed to durations of 0.7 ± 0.3 ps in a grating pair arrangement (gratings with 600 grooves mm^{-1}, grating distance 25 cm, angle of incidence 30°, operation in -1st diffraction order).

Here the intracavity self-phase modulation in the Nd:glass laser oscillator and the pulse compression in the grating pair compressor are analysed theoretically. The spectral shapes of the self-phase modulated pulses and the temporal shapes of the compressed pulses are determined by fast-Fourier transformations. The numerical simulations reproduce the experimental findings. The theory presented is generally applicable to self-phase modulation and grating pair pulse compression.

2. Theory

The intracavity self-phase modulation and the grating pair pulse compression are described.

2.1. Intracavity self-phase modulation

The self-phase modulation of a laser pulse is due to temporal refractive index changes caused by the pulse. The refractive index variation comprises electronic contributions (electronic optical Kerr effect), molecular orientational contributions (orientational optical Kerr effect), electrostrictive contributions in solids and thermal contributions [23, 24]. Temporal refractive index changes also occur in saturable absorbers, due to absorption saturation and in active laser media due to gain depletion [2, 25, 26]. In a Nd:glass laser the self-phase modulation is mainly due to the nonlinear electronic refractive index contribution of the laser rod. Only this instantaneous refractive variation, which is proportional to the laser intensity, is considered here.

The refractive index is given by

$$n = n_0 + (n_2/2)|E(t)|^2 = n_0 + \gamma I(t) \tag{1}$$

where n_0 is the linear refractive index of the laser rod at the laser frequency $\nu_0 = \omega_0/2\pi$, n_2 is the field coefficient and γ is the intensity coefficient of the nonlinear refractive index, E is the electric field and I is the intensity of the laser pulse. The relationship between the temporal laser intensity and the temporal electric field strength is

$$I(t) = (n_0 c_0 \varepsilon_0/2)|E(t)|^2 \tag{2}$$

where c_0 is the speed of light in vacuum and ε_0 is the permittivity of vacuum. The relationship between n_2 and γ is $\gamma = n_2/n_0 c_0 \varepsilon_0$.

The wave propagation of the electrical laser field is given by

$$E(t, z) = E_0(t, z) \exp\left[\mathrm{i}(\omega_0 t - kz - \phi_0)\right] \tag{3}$$

where E_0 is the electrical field amplitude, ω_0 is the angular carrier frequency, k is the wavevector, t is the time and z is the spatial coordinate in the propagation direction. ϕ_0 is an initial constant phase which may be set to zero.

The wavevector is given by

$$k = n\omega_0/c_0 = [n_0 + \gamma I(t)]\omega_0/c_0 \tag{4}$$

Using the transformation $t' = t - n_0 z/c_0$, Equation 3 becomes

$$E(t', z) = E_0(t', z) \exp\{i[\omega_0 t' - \gamma(\omega_0/c_0)I(t')z - \phi_0]\} \tag{5a}$$

$$= E_0(t', z) \exp\{i[\omega_0 t' - \phi(t', z) - \phi_0]\} \tag{5b}$$

$$= E_0(t', z) \exp\{i[\omega(t')t' - \phi_0]\} \tag{5c}$$

$$= E_{0,m}(t', z) \exp(i\omega_0 t') \tag{5d}$$

where

$$\phi(t', z) = (\omega_0/c_0)\gamma I(t')z \tag{6}$$

is the temporal laser induced phase,

$$\omega(t') = \omega_0 - \frac{\partial\phi(t', z)}{\partial t'} = \omega_0 + \omega_c(t') \tag{7}$$

is the instantaneous angular frequency and

$$E_{0,m}(t', z) = E_0(t', z) \exp\{-i[\phi(t', z) + \phi_0]\} \tag{8}$$

is the self-phase modulated temporal amplitude.

The momentary laser frequency $\nu(t') = \omega(t')/2\pi$ changes with time. One speaks of frequency sweeping or frequency chirp. The frequency chirp $\nu_c(t')$ is

$$\nu_c(t') = \nu(t') - \nu_0 = -\frac{1}{2\pi}\frac{\partial\phi(t', z)}{\partial t'} = -\frac{\nu_0}{c_0}\gamma z\frac{\partial I(t')}{\partial t'} \tag{9}$$

In temporal regions of $\partial\nu_c/\partial t' > 0$ one speaks of positive frequency chirp or frequency up-chirp, and in regions of $\partial\nu_c/\partial t' < 0$ one speaks of negative frequency chirp or frequency down-chirp.

The temporal pulse intensity distribution $I(t')$ is not changed by self-phase modulation, as is seen by insertion of Equation 5 into Equation 2.

The spectral electrical field strength is obtained from the temporal electric field strength by Fourier transformation:

$$E(\omega, z) = \mathcal{F}[E(t', z) = \int_{-\infty}^{\infty} E(t', z) \exp(-i\omega t')\, dt'$$

$$= \int_{-\infty}^{\infty} E_{0,m}(t', z) \exp[-i(\omega - \omega_0)t']\, dt' \tag{10}$$

The transformation $\omega' = \omega - \omega_0$ leads to

$$E(\omega', z) = \int_{-\infty}^{\infty} E_{0,m}(t', z) \exp(-i\omega' t')\, dt' = \mathcal{F}[E_{0,m}(t', z)]$$

$$= |E(\omega', z)| \exp[i\phi(\omega', z)] \tag{11}$$

The spectral intensity distribution is given by [27]

$$I(\omega', z) = (c_0 n_0 \varepsilon_0/4\pi)|E(\omega', z)|^2 \tag{12}$$

Expressed in wavenumbers, $\tilde{\nu}' = \omega'/2\pi c_0$, the spectral intensity distribution is

$$I(\tilde{\nu}', z) = 2\pi c_0 I(\omega', z) \tag{13}$$

because of the energy conservation relation $\int_{-\infty}^{\infty} I(\omega')\,\mathrm{d}\omega' = \int_{-\infty}^{\infty} I(\tilde{\nu}')\,\mathrm{d}\tilde{\nu}'$. The spectral phase is

$$\phi(\tilde{\nu}', z) = \phi(\omega', z) = \mathrm{Im}\,[E(\omega', z)]/\mathrm{Re}\,[E(\omega', z)] \tag{14}$$

A schematic sketch of an active and passive mode-locked laser oscillator is shown in Fig. 1a. The temporal laser intensity $I(t')$, the frequency chirp $\tilde{\nu}_c$ and the spectral laser intensity distribution $I(\tilde{\nu}')$ of a circulating pulse in the laser oscillator are illustrated in Fig. 1b to d. $I(t')$ is Gaussian shaped. $\tilde{\nu}_c$ is proportional to the time derivative of $I(t')$. The frequency chirp broadens and structures the spectral intensity distribution $I(\tilde{\nu}')$.

The spectral pulse broadening $\Delta\nu_m$ due to self-phase modulation is given approximately by

$$\begin{aligned}\Delta\nu_m &= \nu_{c,\max} - \nu_{c,\min} = \frac{\nu_0}{c_0}\gamma z\left(\left.\frac{\partial I}{\partial t'}\right|_{\max} - \left.\frac{\partial I}{\partial t'}\right|_{\min}\right) \\ &= 2^{1/2}4(\ln 2)^{1/2}\exp\left[(-1/2)\nu_0\gamma z I_0\right]/c_0\Delta t\end{aligned} \tag{15}$$

where I_0 is the pulse peak intensity and Δt is the pulse duration (FWHM). The last equality is valid for Gaussian temporal pulses, $I(t') = I_0 \exp\left[-4(\ln 2)t'^2/\Delta t^2\right]$ [28]. The total

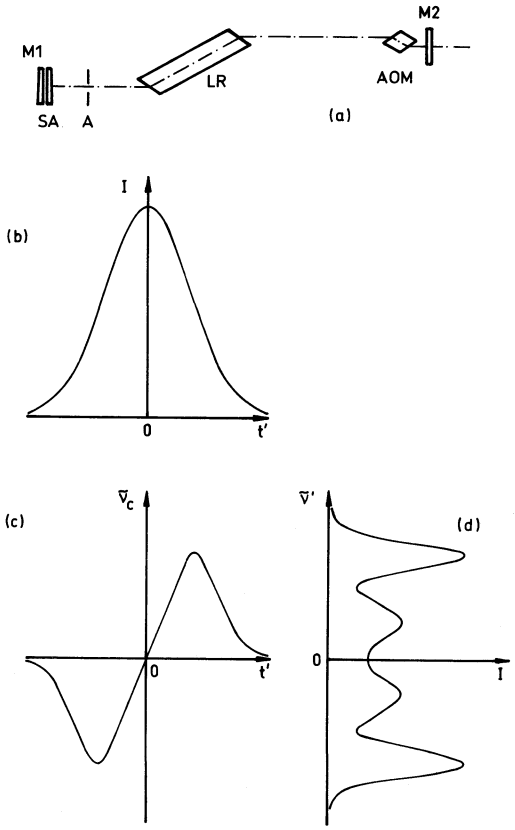

Figure 1 Illustration of intracavity self-phase modulation. (a) Hybridly mode-locked laser system: M1 and M2, laser mirrors; SA, contacted saturable absorber cell; A, aperture; LR, laser rod; and AOM, acousto-optic mode-locker. (b) Temporal shape of circulating laser pulse. (c) Frequency chirp of self-phase modulated pulse. (d) Spectral distribution of self-phase modulated pulse.

spectral width $\Delta\nu$ is given approximately by

$$\Delta\nu = (\Delta\nu_m^2 + \Delta\nu_{bwl}^2)^{1/2} \tag{16}$$

where $\Delta\nu_{bwl}$ is the bandwidth limited spectral width. The relationship between $\Delta\nu_{bwl}$ and Δt is $\Delta\nu_{bwl} = \kappa/\Delta t$ where κ is of the order of unity and depends on the explicit pulse shape. For Gaussian pulses it is $\kappa = 0.441$ [29]. The bandwidth product of self-phase modulated pulses is

$$\Delta\nu\Delta t \approx [(\Delta\nu_m \Delta t)^2 + \kappa^2]^{1/2} \tag{17}$$

In the case of intracavity self-phase modulation the circulating laser pulse passes multiple times through the nonlinear refractive medium. The self-phase modulation effect is accumulative within the photon lifetime $t_{ph} = m_{ph} t_R \approx t_R/\ln(R_{out}^{-1})$ in the laser oscillator, where t_R is the resonator round-trip time, m_{ph} is the number of round-trips within the photon lifetime and R_{out} is the reflectivity of the output mirror. The length z entering the above equations is given by

$$z = 2l(1 + m_{ph}) \approx 2l[1 + 1/\ln(R_{out}^{-1})] \tag{18}$$

where l is the length of the nonlinear refractive index medium (the laser rod length).

Using our experimental parameters of $l = 13$ cm (Nd:glass rod length), $R_{out} = 0.3$, $\tilde{\nu}_0 = \lambda_0^{-1} = 9490\,\text{cm}^{-1}$ ($\lambda_0 = 1054$ nm), $\gamma \approx 4 \times 10^{-16}\,\text{cm}^2\,\text{W}^{-1}$ [30] and $I_0 \approx 10^{10}\,\text{W cm}^{-2}$, a bandwidth product of $\Delta\nu\Delta t \approx 6$ is calculated. For $\Delta t = 5$ ps the spectral width is $\Delta\tilde{\nu} \approx 45\,\text{cm}^{-1}$, a reasonable agreement with our experimental findings [22].

The temporal pulse broadening (transit time spreading, temporal chirp) due to the group velocity dispersion, $v_g = c_0/(n_0 - \lambda_0 \partial n/\partial\lambda_0)$, in the laser rod is approximately given for a

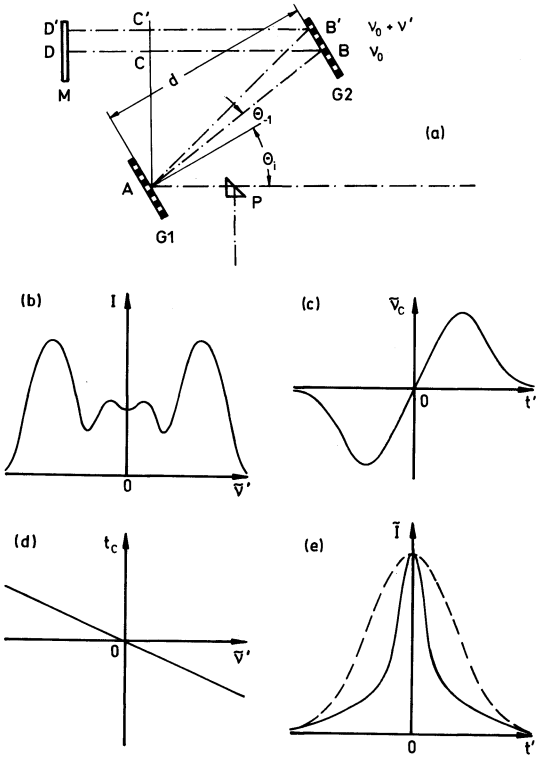

Figure 2 Illustration of grating pair pulse compression. (a) Experimental arrangement: G1 and G2, gratings; M, mirror; and P, deflection prism. (b) Self-phase modulated spectrum. (c) Frequency chirp of self-phase modulated input pulse. (d) Time chirp of grating pair arrangement. (e) Temporal pulse shape of input pulse (broken curve) and output pulse (full curve).

double passage by [2, 31, 32]

$$\delta t_{tr} \approx \frac{\kappa \lambda_0^3 2l}{c_0^2 \Delta t} \left| \frac{\partial^2 n}{\partial \lambda_0^2} \right| \tag{19}$$

A value of $\delta t_{tr} = 3.3\,\text{fs}$ is calculated for our experimental data of $\lambda_0 = 1054\,\text{nm}$, $l = 13\,\text{cm}$, $\Delta t = 5\,\text{ps}$ and $\partial^2 n/\partial \lambda_0^2 = 1.12 \times 10^{-8}\,\text{nm}^{-2}$ (material dispersion parameter $M = (\lambda_0/c_0)\partial^2 n/\partial \lambda_0^2 = 39.3\,\text{ps nm}^{-1}\,\text{km}^{-1}$ [33], dispersion data of Schott glass BK7 are used). The transit time broadening is not accumulative because the broadening is compensated by the pulse shortening in the active and passive mode-locker. The transit time broadening in the Nd : glass laser is negligibly small and is not considered further.

The transit time broadening due to group velocity dispersion is an important pulse duration limiting factor in femtosecond dye lasers [1, 2, 32, 34]. The combined treatment of self-phase modulation (frequency chirp) and group velocity dispersion (time chirp) leads to a more complicated wave propagation equation (nonlinear Schrödinger equation) [1, 2, 16–18].

2.2. Grating pair pulse compression

The geometric layout of a grating pair pulse compressor is shown in Fig. 2a. The input pulse is fanned out at the first grating G1 and parallelized at the second grating G2. The mirror M reverses the ray direction and the spectrally dispersed pulse is fanned in by G2 and parallelized by G1. The different spectral components have different transit times, leading to a temporal chirp of the spectrum (temporal sweep of spectral components across frequency). An initially bandwidth-limited pulse is slightly broadened temporally by the time chirp in the grating pair arrangement (see Fig. 6, below), but a properly frequency up-chirped pulse is compressed (see Fig. 7, below; the leading-pulse front moves more slowly and the trailing pulse front moves faster through the arrangement).

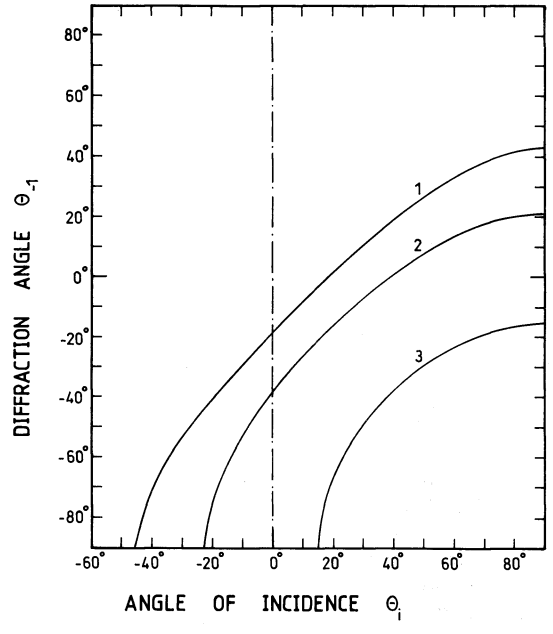

Figure 3 Diffraction of light into −1st order by a grating. The curves are for $\lambda_0 = 1054\,\text{nm}$ and spatial grating frequencies of $g = 300$ (curve 1), 600 (2) and 1200 (3) mm^{-1}. The same curves apply to $\lambda_0' = \lambda_0/b$ and $g' = bg_0$ with b a positive factor. For the definition of angles see Fig. 2a.

The temporal shaping of a positive self-phase modulated pulse (spectrum in Fig. 2b and frequency chirp in Fig. 2c) is illustrated in Fig. 2d and 2e. The time chirp is shown in Fig. 2d. The initial temporal pulse shape is shown by the broken curve and the compressed pulse shape is shown by the full curve in Fig. 2e.

The angular spreading of the input pulse is given by the grating equation [35]

$$a(\sin\theta_m - \sin\theta_i) = m\lambda_0 = mc_0/\nu_0 \tag{20}$$

where $a = g^{-1}$ is the groove spacing (g is the spatial grating frequency in lines mm^{-1}), θ_i is the angle of incidence and θ_m is the diffraction angle. m is the diffraction order.

The diffraction angle θ_{-1} versus angle of incidence θ_i is plotted in Fig. 3. The curves are calculated for three different $\lambda_0 g$ values of 0.3162 (curve 1), 0.6324 (2), and 1.2648 (3) corresponding to g = 300 (1), 600 (2) and 1200 (3) lines mm^{-1} at λ_0 = 1054nm. The negative θ_i angles and corresponding negative θ_{-1} angles are equivalent to positive θ_i angles and positive θ_1 angles (m = 1). The allowed angles of incidence are limited to regions of $|\theta_m| < 90°$. $\theta_i(|\theta_m| = 90°)$ is called the limiting angle $\theta_{i,lim}$. In our experiments we used g = 600 lines mm^{-1}, $m = -1$ and $\theta_i = 30°$, resulting in $\theta_{-1} \approx -8°$.

The path length difference between $\nu = \nu_0 + \nu'$ and ν_0 is

$$\begin{aligned}\Delta L(\nu') &= 2(\overline{AB'} + \overline{B'C'} - \overline{AB} - \overline{BC}) \\ &= 2d\left(\frac{1 + \cos[\theta_i + \theta_m(\nu)]}{\cos[\theta_m(\nu)]} - \frac{1 + \cos[\theta_i + \theta_m(\nu_0)]}{\cos[\theta_m(\nu_0)]}\right)\end{aligned} \tag{21}$$

where d is the distance between the gratings. The time chirp (temporal spread or time lag across frequency) is

$$t_c(\nu') = n_a \Delta L(\nu')/c_0 = \beta(\tilde{\nu}')\tilde{\nu}' d \tag{22}$$

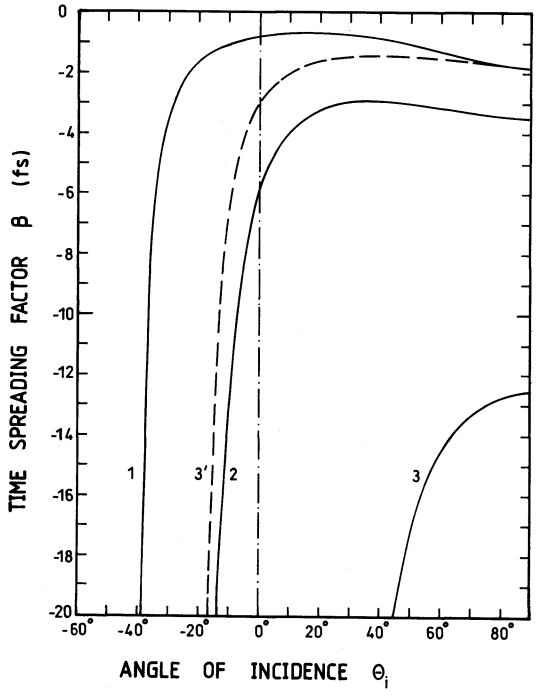

Figure 4 Time spreading factor β in fs $(cm^{-1}\,cm)^{-1}$ versus angle of incidence θ_i. The gratings are operated in −1st diffraction order. Full curves, λ_0 = 1054 nm and broken curve, λ_0 = 527 nm. The curves are for (curve 1) g = 300 mm^{-1}, (2) g = 600 mm^{-1} and (3 and 3') g = 1200 mm^{-1}.

where n_a is the refractive index of air ($n_a = 1$ in our calculations). The last equality defines the time spreading factor $\beta = t_c(\tilde{\nu}')/\tilde{\nu}'d$ (dimension $s(cm^{-1}\,cm)^{-1}$). For $\beta < 0$ we may speak of negative time chirp (temporal down-chirp) and for $\beta > 0$ of positive time chirp (temporal up-chirp).

The time spreading factor β versus angle of incidence θ_i is plotted in Fig. 4 for the -1st diffraction order ($\theta_i < 0$ and $m = -1$ are equivalent to $\theta_i > 0$ and $m = 1$). The full curves are calculated for $\lambda_0 = 1054\,nm$ and spatial grating frequencies of $g = 300$ (curve 1), 600 (2) and 1200 (3) lines mm^{-1}. The broken curve is for $\lambda_0 = 527\,nm$ and $g = 1200$ lines mm^{-1} ($|\beta|$ is a factor of 2 smaller than for $\lambda_0 = 1054\,nm$ and $g = 600$ lines mm^{-1}). The time spreading is rather constant over a wide range of angles of incidence. Towards the limiting angle $\theta_{i,lim}$ it increases strongly and diverges at $\theta_{i,lim}$. The time spreading factor β is negative, i.e. parallel grating pair arrangements give a negative time chirp. The combination of positive frequency chirp and negative time chirp allows temporal pulse compression.

The time spreading factor β across frequency $\tilde{\nu}' = \tilde{\nu} - \tilde{\nu}_0$ is shown in Fig. 5 for $\lambda_0 = 1054\,nm$ and $g = 600$ lines mm^{-1}. The various curves are for different angles of incidence. For $\theta_i \gtrsim 20°$ $\beta(\tilde{\nu}')$ is nearly constant and consequently the time chirp t_c is linear within the shown spectral range from -80 to $80\,cm^{-1}$. The curves for $\theta_i = 0$ and $-10°$

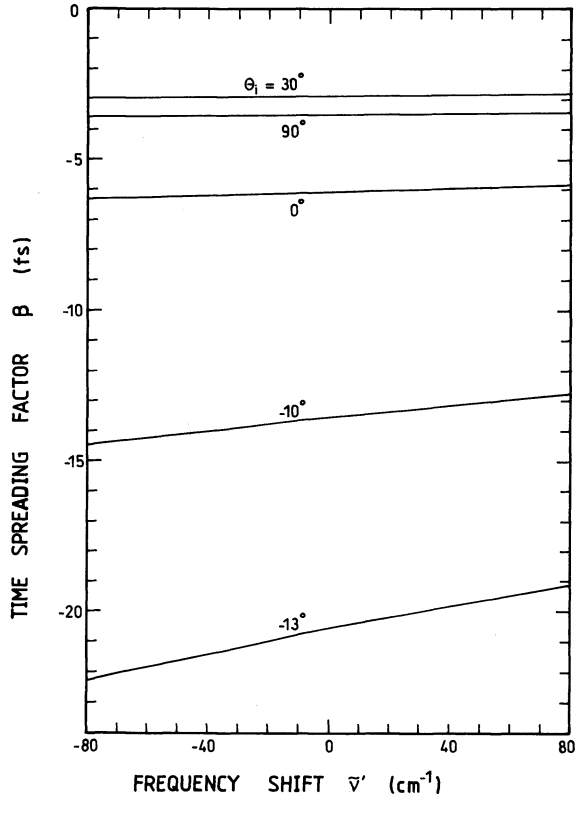

Figure 5 Time spreading factor β versus frequency $\tilde{\nu}' = \tilde{\nu} - \tilde{\nu}_0$. The curves are for the -1st diffraction order, $\lambda_0 = \tilde{\nu}_0^{-1} = 1054\,nm$, and $g = 600\,mm^{-1}$. The angles of incidence are varied for the various curves.

show a linear slope. At $\theta_i = -13°$ the curve shows a slight curvature. Towards the limiting angle $\theta_{i,lim}$ the steepness and the curvature of the curves increase.

The time chirp in the grating pair compressor causes a phase change

$$\phi_g(\omega') = \omega' t_c(\omega') \tag{23}$$

For the frequency region shown in Fig. 5 $\beta(\tilde{\nu}')$ is constant over a wide range of angles of incidence, giving a linear $t_c(\omega')$ and a quadratic $\phi_g(\omega')$. Under our experimental conditions of $\theta_i = 30°$, $\lambda_0 = 1054\,\text{nm}$ and $g = 600\,\text{lines mm}^{-1}$ $\phi_g(\omega')$ is quadratic over the spectral width of the self-phase modulated pulses ($\Delta\tilde{\nu} \approx 60 \pm 20\,\text{cm}^{-1}$). Towards the limiting angle $\theta_{i,lim}$ cubic (linear slope of $\beta(\tilde{\nu}')$) and higher-order contributions of $\phi_g(\omega')$ gain importance. In calculating ϕ_g by use of the Equations 21 to 23, no approximations are made, i.e. all terms in a power expansion of ϕ_g are included.

The grating pair compressor changes the input spectral phase $\phi(\omega')$ to

$$\tilde{\phi}(\omega') = \phi(\omega') + \phi_g(\omega') \tag{24}$$

The electric field strength in the frequency space changes to

$$\tilde{E}(\omega', z) = |E(\omega', z)| \exp[i\tilde{\phi}(\omega')] \tag{25}$$

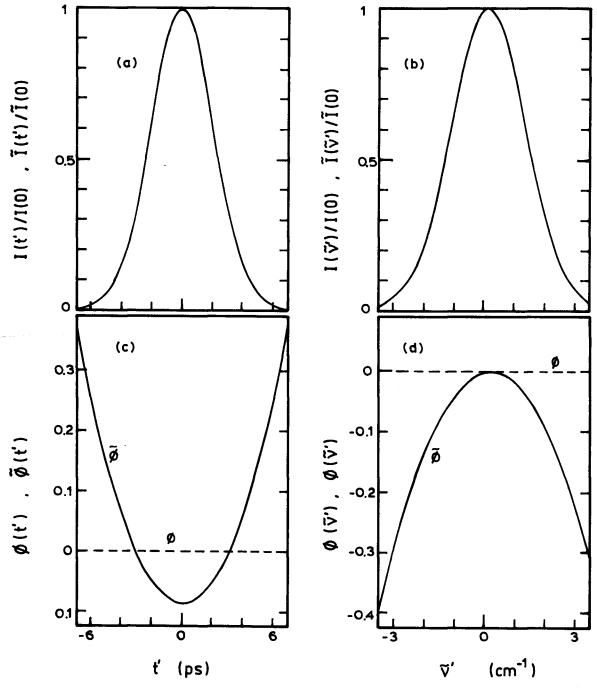

Figure 6 Pulse shaping of frequency unchirped (bandwidth-limited) pulse in a grating pair compressor. $\theta_i = 30°$, $g = 600\,\text{mm}^{-1}$, -1st order, $\lambda_0 = 1054\,\text{nm}$, $\phi_{max} = 0$; $\Delta t = 5\,\text{ps}$ and Gaussian shape, $d = 3.2\,\text{m}$. (a) Input and output pulse shape (no observable difference). (b) Input and output spectrum (identical). (c) Temporal input phase $\phi(t')$ and output phase $\tilde{\phi}(t')$. (d) Spectral input phase $\phi(\tilde{\nu}')$ and output phase $\tilde{\phi}(\tilde{\nu}')$.

while the spectral intensity distribution remains unchanged, i.e.

$$\tilde{I}(\omega', z) = I(\omega', z) \tag{26}$$

(see Equation 12).

The amplitude $\tilde{E}_0(t', z)$ of the temporal electrical field strength behind the compressor, $\tilde{E}(t', z) = \tilde{E}_0(t', z) \exp(i\omega_0 t')$ is obtained by inverse Fourier transformation

$$\tilde{E}_0(t', z) = \mathscr{F}^{-1}[E(\omega', z)] = |\tilde{E}_0(t', z)| \exp[-i\tilde{\phi}(t')] \tag{27}$$

The reshaped temporal pulse intensity is given by

$$\tilde{I}(t', z) = (n_0 \varepsilon_0 c_0/2)|\tilde{E}_0(t', z)|^2 \tag{28}$$

and the temporal output phase is

$$\tilde{\phi}(t') = -\operatorname{Im}[\tilde{E}_0(t', z)]/\operatorname{Re}[\tilde{E}_0(t', z)] \tag{29}$$

The pulse duration Δt_{out} behind the grating pair pulse compressor may be estimated by

$$\Delta t_{out} \approx (\kappa/\Delta\nu) + |\Delta t - (\kappa/\Delta\nu) + \beta d\Delta\tilde{\nu}| \tag{30}$$

($\kappa = 0.441$ for Gaussian pulses). The shortest output pulse duration is expected when the

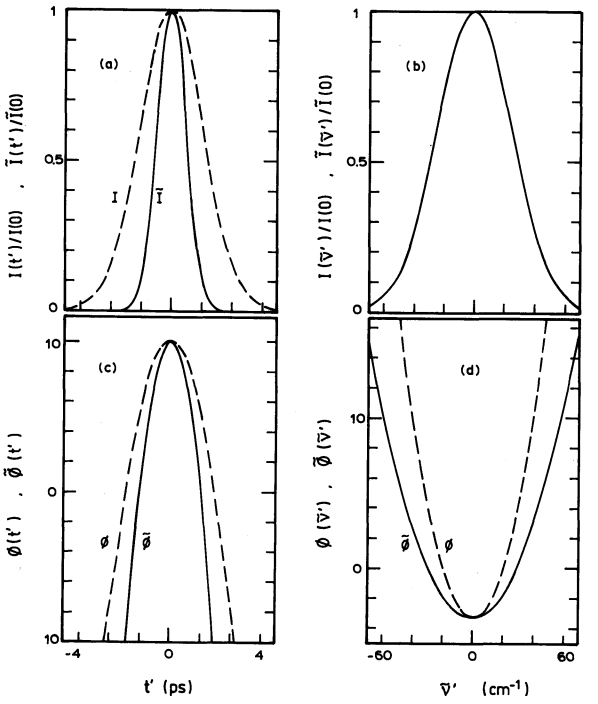

Figure 7 Pulse shaping of linearly frequency up-chirped pulse in grating pair compressor. $\theta_i = 30°$, $g = 600\,\mathrm{mm}^{-1}$, -1st order, $\lambda_0 = 1054\,\mathrm{nm}$, $\phi_{max} = 10$, $\Delta t = 5\,\mathrm{ps}$. (a) Input $I(t')$ and output $\tilde{I}(t')$ pulse shape. (b) Input and output spectrum (identical). (c) Temporal input phase $\phi(t')$ and output phase $\tilde{\phi}(t')$. (d) Spectral input phase $\phi(\tilde{\nu}')$ and output phase $\tilde{\phi}(\tilde{\nu}')$. The same curves are obtained for $\theta_i = -13°$ and $d = 7\,\mathrm{cm}$.

second term of Equation 30 vanishes. For $\Delta t = 5\,\text{ps}$, $\Delta\tilde{\nu} = 60\,\text{cm}^{-1}$ and $\beta = -2.9 \times 10^{-15}\,\text{s}$ (Fig. 4) an optimum grating distance of $d = 27\,\text{cm}$ is estimated. In the experiments $d = 25\,\text{cm}$ was used [22].

3. Numerical simulations

The spectral shaping of Gaussian pulses and Gaussian cosine modulated pulses due to self-phase modulation and the temporal shaping of self-phase modulated pulses in a grating pair compressor are simulated. The Fourier transforms are performed on a mainframe computer applying the NAG routine C06ECF.

The uncompressed temporal pulse shape is set to

$$\frac{I(t')}{I(0)} = \exp(-t'^2/t_0^2)[1 + A\cos(\pi t'/t_{\text{mod}})]/(1 + A) \tag{31}$$

$t_0 = \Delta t/2(\ln 2)^{1/2}$ is half the 1/e pulsewidth of the Gaussian envelope. t_{mod} gives the temporal modulation spacing and A determines the modulation depth. For $A = 0$ Equation 31 represents a Gaussian shape.

The uncompressed temporal phase is (see Equation 6)

$$\phi(t') = \phi_{\max} I(t')/I_{\max} \tag{32}$$

with

$$\phi_{\max} = (\omega_0/c_0)\gamma z I_{\max} \tag{33}$$

ϕ_0 is set to zero. For $\phi_{\max} > 0$ ($\gamma > 0$) one speaks of positive self-phase modulation. In this

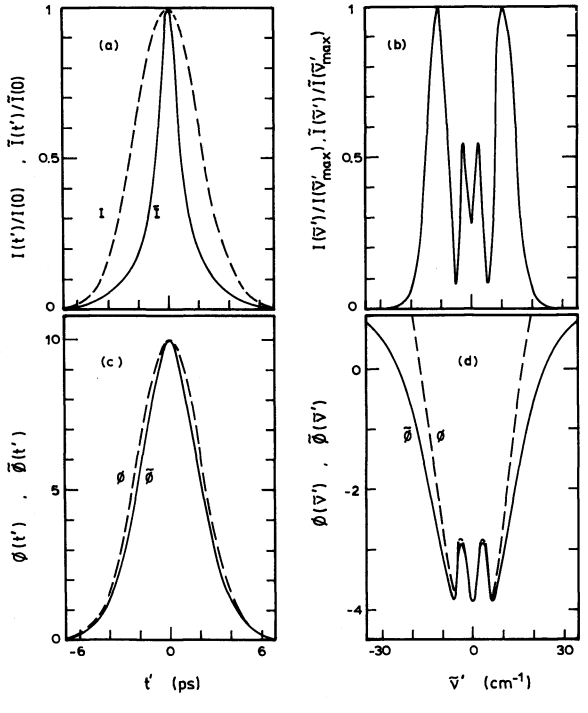

Figure 8 Pulse shaping of positive self-modulated pulse in a grating pair compressor. For legend see Fig. 7.

case the pulses are mainly frequency up-chirped (positive frequency chirp, $\partial\nu_c/\partial t' > 0$, at central part of the pulse, see Fig. 1). For $\phi_{max} < 0$ ($\gamma < 0$) one would speak of negative self-phase modulation.

The simulations are carried for the fixed parameters of $\lambda_0 = \tilde{\nu}_0^{-1} = 1054\,\text{nm}$, $\Delta t = 5\,\text{ps}$, $g = a^{-1} = 600\,\text{mm}^{-1}$ and $\theta_i = 30°$ (−1st diffraction order). Gaussian pulses ($A = 0$) and completely cosine-modulated Gaussian pulses ($A = 1$, $t_{mod} = 2.5\,\text{ps}$) are considered. The maximum temporal phase ϕ_{max} and the grating distance d are varied.

The influence of the grating pair compressor on a bandwidth-limited Gaussian pulse ($\phi(t') = 0$) is shown in Fig. 6. The grating distance is set to $d = 3.2\,\text{m}$. The time chirp of the compressor is seen by the quadratic phase $\tilde{\phi}(\tilde{\nu}') = \phi_g(\tilde{\nu}')$ (see Equation 23). It causes a slight pulse broadening of $\Delta t_{out}/\Delta t = 1.015$ which is too small to be visible in Fig. 6a. The spectral intensity distribution (Fig. 6b) is not modified in the compressor (see Equation 26). The temporal phase $\tilde{\phi}(t')$ behind the compressor is shown in Fig. 6c.

In a first-order discussion of frequency chirping by self-phase modulation the chirp is linearized, i.e. for a temporal Gaussian pulse shape the phase $\phi(t') = \phi_{max} \exp(-t'^2/t_0^2)$ is approximated by

$$\phi(t') = \phi_{max}(1 - t'^2/t_0^2) \tag{34}$$

leading to a frequency chirp of

$$\nu_c(t') = (1/\pi)\phi_{max} t'/t_0^2 \tag{35}$$

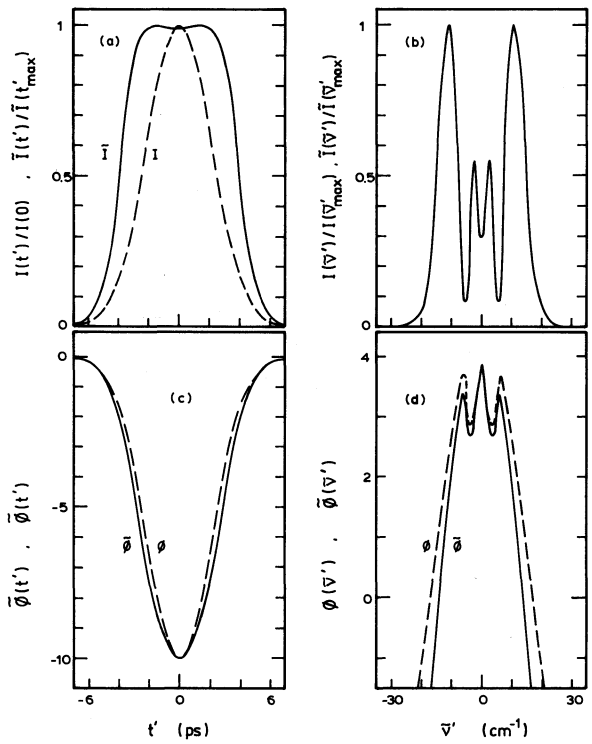

Figure 9 Pulse shaping of negative self-modulated pulse in the grating pair arrangement. The legend of Fig. 7 applies except $\phi_{max} = -10$.

The pulse shaping in the linearized approximation is illustrated in Fig. 7 for $\phi_{max} = 10$ and $d = 0.5$ m. The spectrum of the linear frequency chirped pulse is broadened but the spectral shape is unchanged. The bandwidth product is $\Delta\nu\Delta t = 10.9$. The quadratic temporal phase $\phi(t)$ causes a quadratic spectral phase $\phi(\tilde{\nu}')$ (Fig. 7d). The practically linear time chirp of the grating pair compressor lowers the phases $\tilde{\phi}(\tilde{\nu}')$ and $\tilde{\phi}(t')$. For the spectral phase the curvature at $\tilde{\nu}' = 0$ is reduced, whereas for the temporal phase the curvature at $t' = 0$ is increased. The output pulse is temporally compressed (Fig. 7a) but it remains its temporal shape. For the intracavity self-phase modulated laser of Fig. 1 only the central part of the pulses is described well by linear frequency chirping. A good linear chirp over nearly the whole pulse is achieved by the combined effect of self-phase modulation and group velocity dispersion in fibres [1, 2, 16, 17].

The influence of deviations from the linear time chirp of the grating pair compressor near the limiting angle of incidence on the pulse shaping was calculated for $\theta_i = -13°$ and $d = 7$ cm (see Fig. 5, t_c is kept constant). The cubic contribution to $\phi_g(\tilde{\nu}')$ is still too small to have an observable influence on the compressed pulse parameters $\tilde{\phi}(\tilde{\nu}')$, $\tilde{\phi}(t')$ and $\tilde{I}(t')$.

The pulse shaping of positive self-phase modulated Gaussian pulses is illustrated in Fig. 8 ($\phi_{max} = 10$, $d = 0.5$ m). The pulse spectrum is modulated and broadened. The bandwidth product is $\Delta\nu\Delta t = 4.5$. The $\phi(\tilde{\nu}')$ curve is modulated around $\tilde{\nu}' = 0$ with nearly

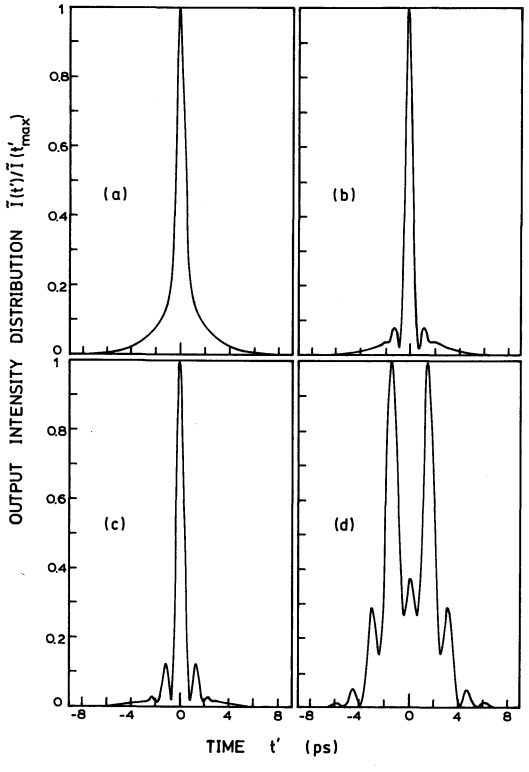

Figure 10 Temporal shapes of positive self-phase modulated Gaussian pulses ($\Delta t = 5$ ps and $\phi_{max} = 10$ giving $\Delta\nu\Delta t = 4.48$) behind compressor with gratings of 600 lines mm^{-1}. Grating distances are (a) $d = 0.8$ m, (b) $d = 1.2$ m, (c) $d = 1.6$ m and (d) $d = 3.2$ m.

quadratic wings. The time chirp in the grating pair lowers the values of the phases ($\tilde{\phi}(\tilde{\nu}') < \phi(\tilde{\nu}')$, $\tilde{\phi}(t') < \phi(t')$). The output pulse is temporally compressed in the central region while the temporal wings remain broad.

The influence of deviations from linear time chirp (quadratic dispersion) was calculated. First, calculations were made for $\beta(\tilde{\nu}', \theta_i) = \beta(0, 30°) = -2.9 \times 10^{-15}$ s = constant and $d = 0.5$ m. The curves in Fig. 8 remained unchanged. Then calculations were performed for $\beta(\tilde{\nu}', \theta_i) = \beta(\tilde{\nu}', -13°)$ and $d = 7$ cm. Again the curves in Fig. 8 remained unchanged (slight difference in $\tilde{\phi}(\tilde{\nu}')$ for $|\tilde{\nu}'| > 30\,\text{cm}^{-1}$). The grating pair compressor is described well by a linear time chirp (quadratic dispersion).

For completeness the pulse shaping of a negative self-phase modulated Gaussian pulse is displayed in Fig. 9. The applied parameters are $\phi_{max} = -10$ and $d = 0.5$ m. The spectral intensity distribution $I(\tilde{\nu}')$ (Fig. 9b) is identical to Fig. 8b. The phase $\phi(\tilde{\nu}')$ has opposite sign. Again the grating pair lowers the values of the phases. The output pulse is temporarily broadened (Fig. 9a).

The influence of the grating distance d on the temporal pulse shaping of a positive self-phase modulated Gaussian pulse is studied in Fig. 10. The phase modulation is set to

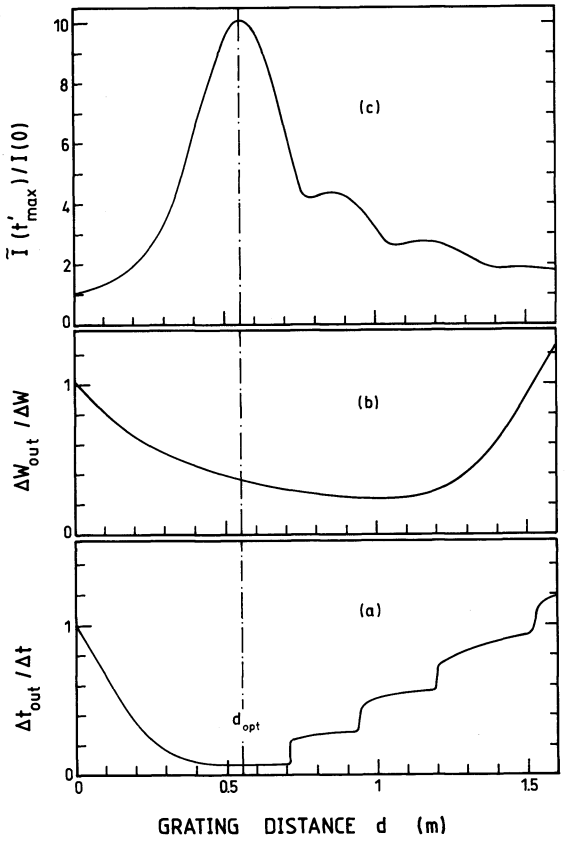

Figure 11 Compression behaviour of positive self-phase modulated Gaussian pulses as a function of grating distance for $\Delta\nu\Delta t = 10$. (a) Pulse compression $\Delta t_{out}/\Delta t$. (b) Energy ratio outside central halfwidth $\Delta W_{out}/\Delta W$. (c) Intensity enhancement $\tilde{I}(t'_{max})/I(0)$.

$\phi_{max} = 10$. From Fig. 10a to d the grating distance is increased. First the central part of the pulse narrows, then it breaks up in more and more subpulses. Beyond a certain grating distance the temporal halfwidth of the pulse envelope Δt_{out} becomes wider than the input pulse duration Δt.

Characteristic pulse shaping parameters of a positive self-phase modulated pulse ($\phi_{max} = 22.3$, corresponding to $\Delta\nu\Delta t = 10$) are shown in Fig. 11 as a function of grating distance. Fig. 11a shows $\Delta t_{out}/\Delta t$. Up to an optimum grating distance, d_{opt}, the pulse shortening increases continuously. Beyond d_{opt}, $\Delta t_{out}/\Delta t$ increases in steps whenever subspikes in the wings grow beyond half the maximum pulse height. The ratio of pulse energy $\Delta W_{out}/\Delta W$ outside the temporal halfwidth Δt is shown in Fig 11b. ΔW_{out} and ΔW are defined by

$$\Delta W_{out} = \int_{-\infty}^{-\Delta t/2} \tilde{I}(t')\,dt' + \int_{\Delta t/2}^{\infty} \tilde{I}(t')\,dt' \tag{36a}$$

and

$$\Delta W = \int_{-\infty}^{-\Delta t/2} I(t')\,dt' + \int_{\Delta t/2}^{\infty} I(t')\,dt' \tag{36b}$$

The energy concentration to the pulse centre continues beyond d_{opt}, but for very large grating distances the energy flows out to the spikes in the wings. The pulse shortening is accompanied by an increase of the output peak intensity $\tilde{I}(t'_{max})$ as is shown in Fig. 11c.

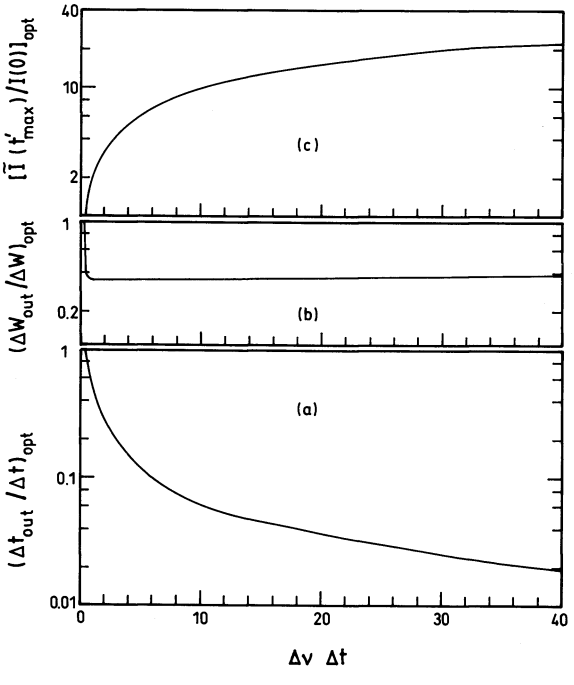

Figure 12 Compression behaviour of positive self-phase modulated Gaussian pulses versus bandwidth product $\Delta\nu\Delta t$ in the case of optimum grating distance $d = d_{opt}$. (a) $(\Delta t_{out}/\Delta t)_{opt}$, (b) $(\Delta W_{out}/\Delta W)_{opt}$ and (c) $[\tilde{I}(t'_{max})/I(0)]_{opt}$.

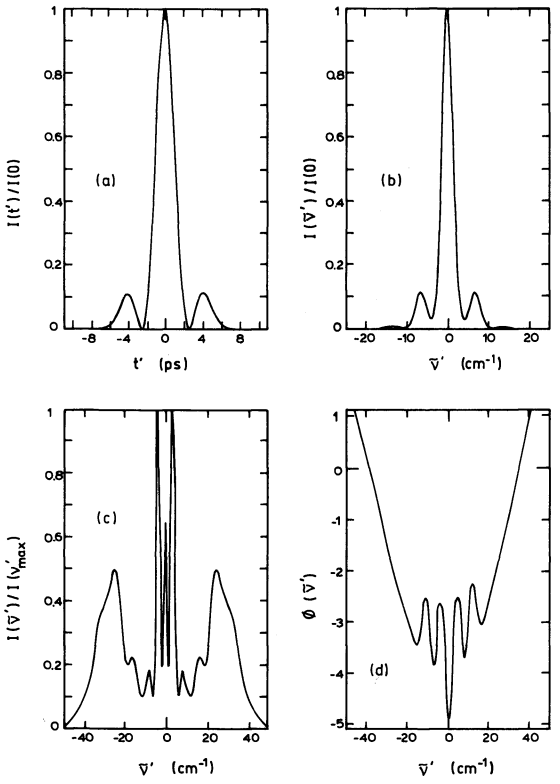

Figure 13 (a) Temporal shape of input cosine-modulated Gaussian pulse. Δt = 5 ps, t_{mod} = 2.5 ps and A = 1 (Equation 31). The shape is independent of self-phase modulation. (b) Spectrum of bandwidth-limited pulse of (a). (c) Spectrum of self-phase modulated pulse of (a) with ϕ_{max} = 10. The shape is independent of compression. (d) Spectral phase of self-phase modulated input pulse (a) with ϕ_{max} = 10.

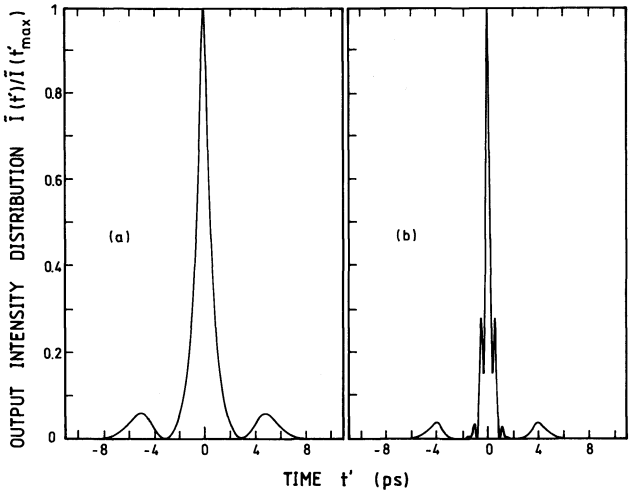

Figure 14 Temporal shapes of the positive self-phase modulated pulses of Fig. 13a, c and d (ϕ_{max} = 10) behind the compressor. Grating distances are (a) d = 0.2 m and (b) d = 0.4 m (g = 600 lines mm^{-1}).

The parameters $\Delta t_{out}/\Delta t$, $\Delta W_{out}/\Delta W$ and $\tilde{I}(t'_{max})/I(0)$ at d_{opt} are displayed versus the bandwidth product $\Delta\nu\Delta t$ in Fig. 12. The pulse shortening and the rise of peak pulse intensity continue with increasing bandwidth product. The pulse energy ratio $\Delta W_{out}/\Delta W$ in the wings is nearly independent of the bandwidth product.

In our experiments intracavity self-phase modulated pulses at $\Delta t = 5\,\text{ps}$ and $\Delta\tilde{\nu} \approx 70\,\text{cm}^{-1}$ ($\Delta\nu\Delta t \approx 10$) could be compressed to $\Delta t_{out} \approx 0.7\,\text{ps}$ ($\Delta t_{out}/\Delta t \approx 0.14$) using a grating distance of $d = 25\,\text{cm} \approx d_{opt}/2$. These experimental results are in reasonable agreement with the theoretical results of Figs 11 and 12.

The pulse shaping of cosine-modulated Gaussian pulses is shown in Figs 13 and 14. The input temporal shape $I(t')$ is shown in Fig. 13a. The corresponding bandwidth-limited spectrum is displayed in Fig. 13b. The self-phase modulation spectrum for $\phi_{max} = 10$ is shown in Fig. 13c. Compared with the temporal Gaussian pulse shape, energy is concentrated in the spectral centre. The phase $\phi(\tilde{\nu}')$ of the self-phase modulated pulse is plotted in Fig. 13d. Examples of compressed pulse shapes are given in Fig. 14a and b for two different grating distances. Again the pulses narrow and then break up into subspikes.

In the experiments both kinds of spectral shapes, like those presented in Figs 8b and 13c, have been observed. The temporal pulse modulation, corresponding to the spectral shape of Fig. 13c, is thought to be due to the combined action of self-phase modulation and spectral hole burning towards the end of the pulse train in the inhomogeneously broadened Nd : glass gain medium [9, 36].

4. Conclusions

The spectral pulse shaping by intracavity self-phase modulation and the temporal pulse shaping of the self-phase modulated pulses in a grating pair compressor have been studied theoretically by Fourier transform analysis. The intracavity self-phase modulation broadens and structures the pulse spectra but does not change the pulse duration. On the other hand, the grating pair compressor does not modify the pulse spectrum but changes the temporal pulse shape and results in a pulse compression for proper grating distances.

The pulse parameters and grating pair parameters applied in the simulations were selected to simulate our recent experiment of the compression of intracavity self-phase modulated pulses of a hybridly mode-locked Nd : glass laser [22]. However, the results are quite general and apply to the self-phase modulation and grating pair pulse compression of other laser systems as well, if group velocity dispersion in the self-phase modulation medium is negligible.

Acknowledgements

The author thanks W. Scheidler for cooperation in the experimental pulse compression studies, and the Rechenzentrum of the University of Regensburg for the allocation of computer time.

References

1. A. M. JOHNSON and C. V. SHANK, in 'The Supercontinuum Laser Source', edited by R. R. Alfano (Springer-Verlag, New York, 1989) p. 399.
2. W. RUDOLPH and B. WILHELMI, 'Light Pulse Compression' (Harwood, London, 1989).

3. M. PESSOT, J. SQUIER, P. BADO, G. MOUROU and D. J. HARTER, *IEEE J. Quantum Electron.* **QE-25** (1989) 61.
4. O. E. MARTINEZ, *ibid.* **QE-24** (1988) 2530.
5. A. M. WEINER, J. P. HERITAGE and E. M. KIRSCHNER, *J. Opt. Soc. Am.* **B5** (1988) 1553.
6. A. M. WEINER, D. E. LEAIRD, J. S. PATEL and J. R. WULLERT, in 'Ultrafast Phenomena VII', edited by C. B. Harris, E. P. Ippen and A. Zewail, Springer Series in Chemical Physics, Vol. 53 (Springer-Verlag, Berlin, 1990) p. 166.
7. A. PENZKOFER and F. GRAF, *Opt. Quantum Electron.* **17** (1985) 219.
8. D. VON DER LINDE and A. M. MALVEZZI, *Appl. Phys.* **B37** (1985) 1.
9. P. SPERBER and A. PENZKOFER, *Opt. Commun.* **54** (1985) 160.
10. J. SCHMIDT, F. REIL and A. PENZKOFER, *ibid.* **58** (1986) 427.
11. T. TOMIE, *Jpn. J. Appl. Phys.* **24** (1985) 1008.
12. A. S. L. GOMES, A. A. GOUVEIA-NETO, J. R. TAYLOR, H. AVRAMOPOULOS and G. H. C. NEW, *Opt. Commun.* **59** (1986) 399.
13. D. J. BRADLEY, in 'Ultrashort Light Pulses', edited by S. L. Shapiro, Topics in Applied Physics, Vol. 18 (Springer-Verlag, Berlin, 1977) p. 1.
14. W. H. LOWDERMILK, in 'Laser Handbook', Vol. 3, edited by M. L. Stitch (North-Holland, Amsterdam, 1979) Ch.B1.
15. L. YAN, J.-D. LING, P.-T. HO, C. H. LEE and G. L. BURDGE, *IEEE J. Quantum Electron.* **24** (1988) 418.
16. G. P. AGRAWAL, 'Nonlinear Fiber Optics' (Academic Press, Boston, 1989).
17. A. HASEGAWA, 'Optical Solitons in Fibers', Springer Tracts in Physics, Vol. 116 (Springer-Verlag, Berlin, 1989).
18. L. F. MOLLENAUER, R. H. STOLEN and J. P. GORDON, *Phys. Rev. Lett.* **45** (1980) 1095.
19. J. A. VALDMANIS, R. L. FORK and J. P. GORDON, *Opt. Lett.* **10** (1985) 131.
20. J. HEPPNER and J. KUHL, *Appl. Phys.* **47** (1985) 453.
21. M. YAMASHITA, K. TORIZUKA and T. SATO, *IEEE J. Quantum Electron.* **QE-23** (1987) 2005.
22. W. SCHEIDLER and A. PENZKOFER, *Opt. Commun.* **80** (1990) 127.
23. Y. R. SHEN, 'The Principles of Nonlinear Optics' (Wiley, New York, 1984).
24. O. SVELTO, *Prog. Optics* **12** (1974) 1.
25. S. DE SILVESTRI, P. LAPORTA and O. SVELTO, *IEEE J. Quantum Electron.* **QE-20** (1984) 553.
26. O. E. MARTINEZ, R. L. FORK and J. P. GORDON, *J. Opt. Soc. Am.* **B2** (1985) 753.
27. A. PENZKOFER and W. KAISER, *Opt. Quantum Electron.* **9** (1977) 315.
28. B. MEIER and A. PENZKOFER, *Appl. Phys.* **B49** (1989) 513.
29. E. P. IPPEN and C. V. SHANK, in 'Ultrashort Light Pulses', edited by S. L. Shapiro, Topics in Applied Physics, Vol. 18 (Springer-Verlag, Berlin, 1977) p. 83.
30. A. PENZKOFER, *Prog. Quantum Electron.* **12** (1988) 291.
31. A. E. SIEGMAN, 'Lasers' (Oxford University Press, Oxford, 1986) Ch. 9.
32. A. PENZKOFER and W. BÄUMLER, *Opt. Quantum Electron.* **23** (1991) 439.
33. P. L. BOCKO and J. R. GANNON, in 'Handbook of Laser Science and Technology', Vol. V: 'Optical Materials: Part 3, edited by M. J. Weber (CRC Press, Boca Raton, Florida) p. 3.
34. J. C. DIELS, in 'Dye Laser Principles with Applications', edited by F. J. Duarte and L. W. Hillman (Academic Press, Boston, 1990) p. 41.
35. E. P. TREACY, *IEEE J. Quantum Electron.* **QE-5** (1969) 454.
36. A. PENZKOFER and N. WEINHARDT, *ibid.* **QE-19** (1983) 567.